Propagation and hindered settling of laboratory ash flows

L Girolami, T. Druitt, Olivier Roche, Z. Khrabrykh

Propagation and hindered settling of laboratory ash flows

L.Girolami*, T.H. Druitt, O. Roche and Z. Khrabrykh

Laboratoire Magmas et Volcans, Université Blaise Pascal, CNRS et IRD

5 rue Kessler, 63038 Clermont-Ferrand

* Corresponding Author

Abstract

The fluidal behaviour of pyroclastic flows is commonly attributed to high gas pore pressures and associated fluidization effects. We carried out experiments on flows of fluidized volcanic ash at 170° C, which is hot enough to reduce cohesive effects of moisture. The flows were generated in a 3-m-long, horizontal lock-exchange flume. The ash was fluidized and expanded uniformly in the flume reservoir by up to 43 % above loose packing, then released. Each flow defluidized progressively down the flume until motion ceased. Initial expansion (E) and initial height (h_0) were varied independently of one another. The flows travelled in a laminar manner. Flow fronts exhibited three main phases of transport: (1) a brief initial phase of gravitational slumping, (2) a dominant, approximately constant-velocity phase, and (3) a brief stopping phase. Phase-2 frontal velocities scaled with $\sqrt{gh_0}$, like other types of dam-break flow. Deposition from initially expanded flows took place by progressive sediment aggradation at a rate that was independent of distance and varied only with E. Despite rates of shear up to 80 s^{-1}, aggradation rates were identical to those determined independently, at the same value of E, in quasi-static collapse tests. Sedimentation caused the flows to thin progressively during transit until they ran out of volume. The dynamics were governed to a first order by two dimensionless parameters: (1) the initial aspect ratio h_0/x_0 in the lock reservoir, and (2) the ratio t_{sett}/t_{grav} of two timescales: a particle settling time t_{sett} and a gravitational acceleration time t_{grav}.

Keywords: Explosive volcanism, Pyroclastic flows, Sedimentation, Laboratory experiments, Lock-exchange flume, Volcanic ash, Scaling laws.

Introduction

Pyroclastic flows are an important hazard around active volcanoes, and a quantitative understanding of their dynamics is needed. Although observations and approximate measurements of frontal velocities exist [e.g., *Hoblitt,* 1986; *Levine and Kieffer*, 1991; *Loughlin et al.,* 2002], the serious hazards involved preclude more detailed study. Moreover, to date no attempt has been made to generate pyroclastic flows on a laboratory scale under controlled conditions amenable to quantitative study.

This paper concerns those pyroclastic flows that travel as dense granular avalanches with bulk densities less than, but comparable to, those of their deposits [*Sparks,* 1976; *Druitt* 1998; *Branney and Kokelaar*, 2002]. The ability of such flows to travel on slopes much less than the static friction angle of the hot debris is attributed principally to non-equilibrium gas pore pressures and associated fluidization effects [*Sparks*, 1976; 1978; *Wilson*, 1980]. Vertical gas flux reduces friction by counteracting gravity, resulting in partial or total support of particle weight. If the gas velocity is high enough, long-lived particle contacts are disrupted and friction is lost. Possible gas sources include air entrainment, internal production, or gas inherited from source [Wilson, 1980]. As the sources wane, the flow de-fluidizes to form a deposit. Quantification of deposition rates is an essential step in the development of mathematical models of pyroclastic flows.

We have studied the dynamics of rapid shear flows of hot volcanic ash in a laboratory lock-exchange flume. The ash was expanded to different degrees by fluidization, then released and allowed to defluidize progressively during flow down the flume. The low permeability resulted in slow gas release, enabling the flows to travel up to almost 3m before ceasing motion. Defluidization took place by progressive re-sedimentation through hindered particle settling at a rate determined by the imposed initial expansion. The experiments enabled us to measure the effects of rapid shear on particle settling and deposition rates during

defluidization, thereby extending the work of *Druitt et al*. [2007] on ash settling in quasi-static beds. We also studied the effects of sedimentation on the flow dynamics, and deduced some governing scalings. Although carried out in the context of pyroclastic flows, the study may also be relevant to other types of geophysical mass flow such as mudflows and lahars.

Fluidization concepts and previous work

Basic fluidization theory is reviewed in several standard texts [e.g., *Rhodes*, 1998; *Fan and Zhu*, 1998]. When a gas is injected vertically at low velocity into a fine-grained granular bed, the flow is dominated by viscous forces and the vertical pressure drop is proportional to velocity. Once the gas velocity exceeds the minimum fluidization value (U_{mf}), drag counterbalances particle weight, the pressure drop becomes independent of velocity, friction is lost, and the bed adopts a liquid-like behaviour. Gas velocity is expressed as the superficial value through the empty container at the temperature of operation. At minimum fluidization it is given by :

$$U_{mf} = \frac{K_{mf}\rho_{mf}g}{\mu} \qquad (1)$$

where K_{mf} is permeability, μ is dynamic gas viscosity, ρ_{mf} is mixture bulk density and g is gravity. When the particles are small and/or of low density, the bed expands uniformly above U_{mf} before the onset of bubbling at the minimum bubbling velocity, U_{mb}. Beds of large and/or dense particles are incapable of uniform expansion and $U_{mb} \approx U_{mf}$. Particles smaller than ~ 30-100 μm show cohesive behaviour due to electrostatic charging, Van der Waals forces, and/or moisture. Being unable to percolate uniformly through the cohesive fines, the gas channels and bed support is not achieved. Channelling is suppressed if the bed is agitated mechanically [*Nezzal et al.,* 1998, *Druitt et al.,* 2004].

If the gas flux through a uniformly expanded bed is cut abruptly, the particles re-sediment under gravity in what is termed a bed-collapse test [*Geldart and Wong,* 1985; *Lettieri et al.,* 2000; *Bruni et al*., 2006]. Hindered settling occurs at a characteristic velocity and a sediment layer accumulates progressively at the base.

Druitt et al. [2004; 2007] fluidized fine-grained (< 4mm) samples of pyroclastic flow materials at temperatures of up to ~ 550° C. They showed that uniform expansion occurred prior to bubbling provided that (1) a rigorous drying procedure was followed, (2) channelling was suppressed by gentle stirring, and (3) the operating temperature exceeded ~ 50° C to avoid the cohesive effects of adsorbed moisture. *Bareschino et al.* [2007] studied the expansion and collapse behaviours of different size cuts of ignimbrite at room temperature and also observed a regime of uniform expansion. They also investigated the effects of shear on bed collapse by shearing the bed between concentric vertical cylinders, and observed that settling was retarded by shear.

Fluidization in rapid shear flows has been much less well studied than in quasi-static beds. *Ishida et al.* [1980] studied the steady flow of continuously gas-fluidized particles in an inclined channel and identified different flow regimes as a function of gas velocity and material properties. *Eames and Gilbertson* [2000] studied continuously fluidized flows of monodisperse, non-cohesive glass beads on a horizontal surface. The flow behaviour and deposit shapes were modelled using depth-averaged equations of motion. They showed that the presence of a fluidizing gas significantly alters the granular flow dynamics. *Gilbertson and Eames* [2003] extended this work using glass beads of two sizes. *Takahashi and Tsujimoto* [2000] carried out experiments on flows of internally fluidized silica sand and developed equations to describe the flow and sedimentation behaviour, the results forming the basis of a mathematical model of pyroclastic flows.

Roche et al. [2002, 2004] studied lock-exchange flows of fluidized glass beads that were first fluidized in a reservoir to various degrees from $<U_{mf}$ to $>U_{mb}$, then released down a flume. Since the base of their flume was impermeable, the flows defluidized progressively during transit until motion ceased. The authors studied the flow behaviour as a function of particle size and initial fluidization state. They found that flows of fine-grained particles travelled further than ones composed of coarser particles (at the same value of U/U_{mf}), which were more permeable and lost gas more readily by bubbling. They also observed that the flows travelled for a large fraction of their runout in a manner similar to inviscid Newtonian fluids [*Rottman and Simpson*, 1983; *Simpson*, 1997]. *Roche et al.* [2005] extended the study to include bidisperse flows. The experimental system of the present paper is based on that of *Roche et al.* [2002, 2004, 2005], but is capable of withstanding temperatures up to 200° C.

Methods and materials

The high-temperature flume

The experiments were carried out in a linear lock-exchange flume built of aluminium and pyrex and capable of withstanding temperatures of up to 200° C (Figure 1). The flume had a 30-cm-long and 50-cm-high rectangular reservoir in which the ash was fluidized and expanded before being released down a 3-m-long horizontal channel. The height and width of the flume were 30cm and 15cm respectively. The gas flux into the windbox was measured by rotameters, then recalculated as velocity at the operating temperature using the reservoir dimensions and the ideal gas law. A three-way valve allowed the incoming gas to be either directed into the windbox, or vented outward, the latter configuration being used to abruptly cut the gas supply during bed collapse. The windbox was separated from the overlying reservoir by a porous plate of mean pore size 17 μm. The windbox and reservoir were both heated by external heating tapes regulated by thermostats. Experiments were carried out with

the reservoir contents and incoming gas at the same temperature. A differential pressure transducer placed at the rear of the reservoir measured the pressure drop across the bed. The reservoir gate had a heat-resistant seal to prevent leakage, a downward-tapering shape to reduce resistance during opening, and a 20-kg counterweight to facilitate opening at a consistently high speed. Opening the gate released the fluidized contents of the reservoir across the impermeable floor of the flume in the manner of a dam break. This formed a fast-moving, but short-lived, shear flow that defluidized progressively until motion ceased.

Experimental ash

The ash was obtained by drying samples of a non-welded ignimbrite from Neschers (France) for 24 hours, then removing particles larger than 250 μm. It contained a broad spectrum of particle sizes, from ~ 1 to 250 μm, and was very similar to sample NES 250 used by *Druitt et al.* [2007]. We found through preliminary 1-D tests in the flume reservoir that fluidization resulted in elutriation of the finest particles, as well as minor vertical segregation. We therefore left the ash bubbling until sufficient fines had been lost that the elutriation rate became negligible, thereby obtaining a slightly fines-depleted material that we used in the following flume experiments (Table 1). The lack of subsequent elutriation enabled us to use the same batch for all experiments, without significant evolution of the grain size distribution (Table 1).

The 1-D expansion and settling behaviour of the ash was studied in the flume reservoir with the gate shut. The operating temperature was fixed at 170° C, which is high enough to avoid the strong cohesive effects of moisture between particles [*Druitt et al.*, 2007]. Even at this temperature, however, the ash remained slightly cohesive, requiring us to stir it gently to avoid channelling immediately prior to each measurement. Expansion was restricted to the non-bubbling state between U_{mf} and U_{mb}. Heights of expanded beds were estimated relative to

the loosely packed state immediately following defluidization. Vertical sampling and sieving showed that no segregation took place during expansion or settling. This is perhaps surprising given the broad range of particle sizes in the ash. However, it is known that even strongly polydisperse suspensions settle without segregation if the particle concentration is high enough, due to a combination of particle-fluid coupling and particle interlocking [*Davies and Kaye,* 1971; *Lockett and Al-Habooby,* 1974; *Druitt,* 1995].

The velocity-expansion relationship was determined by incrementally increasing the gas velocity (Figure 2a). Below U_{mf}, the pressure drop increased linearly and expansion was negligible. Once U_{mf} was reached, nearly full support was achieved and the bed expanded, lost friction and could be stirred. As velocity was increased above U_{mf}, expansion increased up to ~ 45 % at U_{mb} (Figure 2a). A linear fit to the results for $U_{mf} < U < U_{mb}$ gave :

$$E = 60.5\ U + 0.879, \qquad (2)$$

where E is the expanded height at U divided by non-expanded height at U_{mf}, and U is superficial gas velocity in m s^{-1}.

The sedimentation behaviour of the ash was determined by expanding to a known amount, then cutting the gas supply. The resulting hindered settling function was very similar to that of velocity-expansion (Figure 2b). This is expected because the superficial gas velocity necessary to *expand* a bed to a given voidage is equal to the velocity at which that bed *settles* once the gas supply is turned off, provided that the base of the bed is impermeable [*Richardson and Zaki*, 1954]. This is valid for a monodisperse powder, in which all particles settle at the same speed, or for a polydisperse powder if no segregation takes place, as in our ash. In fact owing to the configuration of our apparatus the settling velocities in Figure 2a are slightly underestimated (Appendix 1). However the underestimation lies within the measurement error and does not negate the agreement between the expansion and hindered

settling functions. The loose-packed bulk density of the ash immediately following bed collapse was about 850 kg m^{-3}.

Procedure

The ash was dried at 200° C for 24 hours prior to each experiment, then transferred as quickly as possible (~ 5 min) to the already-hot flume reservoir and stirred to loosen the bed structure. The temperature was 170° C and the reservoir length (x_0) 30cm in all experiments (Figure 1). Once at temperature, the procedure involved (1) stirring the slightly cohesive ash to prevent channelling; (2) stopping stirring and allowing the bed to expand in the non-bubbling state to the maximum value (previously calculated to correspond to the required height); then (3) rapidly opening the gate before channelling set in. In this way was it possible to generate, in a reproducible manner, flows of uniformly fluidized ash of known initial expansion.

Two parameters were varied in the experiments: the initial expanded bed height h_0 and the expansion E, the two being related by $E = h_0/h_{mf}$. In a first series (experiment set 1), E was varied from 1.00 ($U = U_{mf}$) to 1.43 ($U = 3.25\ U_{mf}$), while keeping h_0 constant at 24.8cm (aspect ratio $h_0/x_0 = 0.83$), irrespective of expansion. In a second series (set 2), E was varied over the same range as in set 1, but h_0 was also varied from 17cm to 24.8cm (aspect ratios 0.58-0.83). This was equivalent to keeping the non-expanded height h_{mf} approximately constant. The E = 1.43 experiments of the two series were mutually equivalent, since they had the same values of E and h_0.

For each experiment the entire flume was filmed at 25 frames per second to allow measurement of frontal velocity. The flow was also filmed in detail at 30cm from the lock gate for measurement of sedimentation rate. Following each experiment the deposit thickness was measured every 5cm to construct the longitudinal profile. Grain-size analyses of samples

collected down the flume confirmed that no detectable size segregation took place in the flows.

Three series of repeat experiments were carried out for specific purposes. In one (E = 1.17; set 2), we filmed the flow with five cameras placed regularly down the length of the flume to measure sedimentation rate as a function of distance. In four experiments (1.00, 1.10, 1.17 and 1.35; set 2), we filmed the flows using a high-speed (1000 frames per second) video camera to study the sedimentation process in more detail. In three others (1.10, 1.17 and 1.35; set 2) small buoyant pumices (~ 3cm; 500-800 kg m^{-3}) were added to the reservoir mixture and the flows were filmed from above using five cameras. The pumices served as tracers for reconstructing surface flow trajectories.

Results

General flow behaviour

When released, the fluidized ash flowed down the flume at speeds of up to 2.3 m s^{-1} until defluidization was complete and motion ceased (Figure 3a). Flows of non-expanded or weakly expanded (E < 1.10) ash decelerated rapidly before coming to rest, and motion ceased simultaneously at the rear and front. The more expanded (E > 1.10) flows travelled faster and further, and the motion ceased first at the rear, then at the front.

The initial heights of the flows as they emerged from the reservoir was 0.15-0.20h_0, with no measurable dependence on E. Propagation was observed to take place in three main phases when plotted as graphs of frontal distance (x_f; all distances measured from the lock gate; Figure 1b) versus time (Figure 4): a brief initial ~ 1g acceleration phase lasting 0.1-0.2 s (phase 1), a dominant phase in which the front had an approximately constant velocity (phase 2); and a brief stopping phase lasting 0.1-0.4 s with decelerations of 0.5-1g (phase 3). Phase 2 accounted for 70-80 % of the runout of the flows. As the flows approached their distal limits

they developed wavy surfaces due to the formation of surface instabilities ~1 cm in amplitude (Figure 3d). The flow aspect ratios (mean thickness / length) first decreased very rapidly during runout, then progressively more slowly (Figure 5).

Once the fronts of the more expanded flows had come to rest, a wave of still-fluidized ash approaching from behind broke over the stationary front a few tenths of a second later, extending the distal limit by up to 20 cm (Figure 3e). We refer to this as the 'secondary wave', or flow phase 4. The volumes of material involved in the secondary waves increased with increasing initial expansion, but were always small. All horizontal motion ceased following phase 4.

Runout distances (x_∞) and times (t_∞) for phases 3 and 4 (denoted x_3, t_3 and x_4, t_4) increased with both E and h_0, but the effect of E was greater. For example, an increase in h_0 from 18.5 cm (set 2) to 24.8 cm (set 1) at an expansion of 1.13 increased runout by only 15 %, whereas increasing h_0 from 18.5 cm to 24.8 cm while also expanding up to 1.43 within set 2 increased runout by about 60 %. The distal limit of flow phase 2 (termed x_2) was consistently 80-90 % of the total primary runout (Figure 7). The frontal velocity during phase 2 (U_2) ranged from 1.8 to 2.3m s^{-1} in the initially expanded flows, increasing slightly with both E and h_0 (Figure 6).

The flow fronts of weakly expanded flows differed in cross-sectional shape from those of more expanded ones. At low expansions ($E < 1.10$) they were wedge-shaped (Figure 3b), whereas in the more expanded flows they were steeper and more rounded (Figure 3c) but became more wedge-shaped as the flow approached its distal limit. The greater the initial expansion, the further down the flume a steep front was maintained.

Repeat experiments dosed with buoyant pumiceous tracer particles showed that surface flow trajectories were rectilinear, irrespective of initial expansion (Figure 8a). The absence of surface vorticity (Figure 8a) suggested that the flows travelled in a laminar manner

(only secondary waves exhibit vorticity), with no turbulent motion on a scale much larger than the particles. Lateral velocity gradients on the flow surfaces were weak, indicating slip at the flume walls (Figure 8b). The sidewall boundary layers were ~ 1 cm wide during phases 1 and 2, but increased to a few cm in phase 3.

Ongoing analysis of high-speed video footage taken through the flume sides has confirmed that the flows travelled in a laminar mode. Vertical velocity profiles in the flows were concave-upward, with a no-slip basal boundary at underlying depositional interface (see below). The data will be presented in detail in another paper (*Girolami et al.,* in prep).

Deposits and strandlines

The deposits had thicknesses of less than 10 cm (most < 5 cm), and extended up to 2.8 m from the lock gate (Figure 9). The mean deposit thickness decreased with initial expansion from 4.2 cm to 1.7 cm in set 1, and from 3.0 cm to 1.7 cm in set 2. The deposit aspect ratios decreased strongly with E but were only weakly dependent on h_0, as shown by the near-superposition of curves for experiment sets 1 and 2 (Figure 10).

The flows left two diffuse marks we term 'strandlines' on the pyrex wall of the flume (Figure 11). Video footage enabled us to determine the origins of these strandlines. The upper one was the trace left by the moving flow and its height recorded the maximum level attained at a given location down the flume. It was present in all experiments, irrespective of E. The lower strandline formed by settling of the ash once horizontal motion had ceased, and was only left by flows with E > 1.10. Once motion had ceased at a given location, the material deflated slowly to the loosely packed state, leaving a trace of its former expanded thickness. The lower strandline therefore provided a measure of the distance to which the flow travelled in the expanded state. This distance, called x_e, was comparable to x_2 and exhibited the same

dependence on E and h_0 (Figure 7). This proved that the initially expanded flows remained expanded throughout most of their runout distances.

Sedimentation behaviour

Deposition from the initially expanded flows was observed to take place by progressive aggradation of a basal sediment layer. Aggradation rates were estimated in a set 2 flow with E = 1.17 using five video cameras located along the flume (Figure 12). We measured the time at which the flow front passed each camera, as well as that at which deposition at the same location was complete (following final settling to form the lower strandline). The difference Δt gave the duration of deposit aggradation and allowed us to estimate the mean aggradation speed S from the final deposit thickness H_{dep} ($S = H_{dep}/\Delta t$). The method assumed (1) that deposition started almost immediately after passage of the flow front, and (2) that it proceeded at a constant rate. Ongoing analysis of high-speed video footage supports these assumptions (*Girolami et al.,* in prep). The values of S were used to calculate the settling velocities of particles in the moving flow. The deposit aggradation speed in a re-sedimenting 1-D bed is related by mass balance to the particle settling velocity, V (Appendix 2). Since no segregation of different particle sizes took place in the flows, the settling velocity of the mixture could be characterized by a single value of V, as in a monodisperse suspension. The values of V thus calculated remained approximately constant at ~ 0.5cm s^{-1}, out to at least 1.5m from the lock gate, after which the flow became too thin for precise measurements (Figure 12).

The result showed that it was sufficient to measure the sedimentation rate at a single location down the flume for representative results. We therefore used video footage taken at 30 cm from the lock gate for all our experiments to measure V as a function of E in the

moving flows. The resulting values were indistinguishable, within error, from those measured in the 1-D collapse tests in the flume reservoir with the lock gate closed (Figure 2b).

Summary

The dynamics of the ash flows was well constrained by observations and measurements. The flows were laminar with no large-scale turbulent motions. Initially expanded flows remained expanded throughout most of their runout, but thinned progressively by sedimentation until they ran out of mass. Deposition took place progressively at the flow base at a rate dependent only on the initial expansion, E, and indistinguishable from that in an equivalent 1-D bed collapse. The flow fronts travelled for most of the runout at an approximately constant velocity. Flow behaviour was governed by both E and $h_{0,}$ the two experimental variables. Runout distance, runout duration (Figure 6) and aspect ratio (Figure 10) depended only weakly on h_0, but strongly on E within the limits of the values used in this study. Frontal velocity depended weakly on both parameters (Figure 6).

Discussion

The dynamics of the ash flows was potentially governed by four effects: initial geometry, gravity, sedimentation, and drag. The existence of drag forces in the flows is necessary to explain the rapid decelerations of the stopping phase. The expanded aspect ratio in the reservoir determined the initial conditions. Gravity drove the flows, while drag hindered them. The role of sedimentation was to progressively reduce the flow volume during runout. Once the flows were sufficiently thin, and surface gradients sufficiently low, drag forces brought the fronts rapidly to rest.

In what follows, we restrict discussion to the dynamics of the initially expanded flows ($E > 1.00$) in which sedimentation played an important role. We do not discuss the non-

expanded flows (E = 1.00), which represent a different regime of flow and deposition because sedimentation cannot take place in a non-expanded flow.

Flow motion and drag forces

Gravitational slumping of dam-break flows typically imposes a characteristic velocity of the order ~ $\sqrt{gh_0}$, determined by the conversion of potential to kinetic energy [*Simpson,* 1997; *Hogg,* 2006]. That our ash flows exhibited this behaviour is evident from plotting frontal position (x_f) versus time (t) (Figure 4) in non-dimensional form (Figure 13a). Scaling x_f by x_0 and t by $x_0/\sqrt{gh_0}$ results in a good collapse for flow phase 1 and a reasonable collapse for phase 2, but does not collapse phase 3. This is the scaling governing the behaviour of aqueous gravity currents [*Rottman and Simpson*, 1983] as well as that of flows of fluidized glass beads [*Roche et al.*, 2004]. It implies a non-dimensional frontal velocity of $\xi\sqrt{gh_0}$ for phase 2, where ξ is a constant. Figure 13a shows that while phase 1 motions were governed entirely by initial geometry and gravity, the roles played by sedimentation and drag were non-negligible in phase 2 and dominant in phase 3.

The values of ξ in dam-break systems depend on the nature and magnitudes of any drag forces acting on the flow. Purely inviscid dam breaks in air theoretically have $\xi = 2$, but the value decreases as drag becomes important [*e.g., Mangeney et al.,* 2000; 2004; *Hogg,* 2006]. Drag forces have greatest effect near the front, where the flow is thinnest [*Hogg and Pritchard*, 2004]. The values of ξ in the ash flows ranged from 1.1 to 1.4 (Figure 13b), much less than the theoretical value, showing that drag affected the frontal speed in phase 2. Moreover, the flows were thinning progressively by sedimentation, so that the situation differed from that in dam breaks of pure fluids. We speculate that the observed approximately constant velocities during phase 2 were due to a balance between the effects of gravity,

sedimentation and drag. Sedimentation rate depended on E (appendix 2), as may also the internal drag forces, so the E-dependence of phase 2 velocity may reflect some combined influence of these two effects.

The nature and magnitudes of the drag forces are not well constrained, the possibilities being a combination of basal stress, sidewall friction, and air drag. Estimating the rate of change of momentum during phase 3 shows that a total drag stress of the order of 100-500 Pa was required to explain the observed decelerations. High speed video footage revealed significant vertical velocity gradients in the moving flows [*Girolami et al.,* in prep], proving the existence of a basal stress. The magnitude of sidewall effects is hard to evaluate; the flows slid against the flume sides with only ~1 cm boundary layers during phase 2, but this increased in phase 3. We conclude that both basal and wall stresses may have contributed to the drag force, but that the basal stress probably dominated. Air drag, on the other hand, was probably negligible. The pressure exerted by air on the flow front was of the order $1/2\rho_a u^2$, where ρ_a is the density of air [*Simpson,* 1997] and cannot have exceeded a few Pa.

Dimensional analysis

In order to investigate the roles of sedimentation and drag, we carry out a dimensional analysis using observations to constrain our choice of dimensionless numbers. The system is characterized by six independent parameters: x_0 the reservoir length, h_0 the initial (expanded) height, E the initial expansion, $\rho_0(E)$ the (expanded) bulk density, g the gravitational acceleration, and an unspecified parameter characterizing the drag force. The hindered settling velocity V(E) is not included, since it is defined uniquely by equation 2. ρ_0 is related to the non-expanded ash density, ρ_{mf}, by $\rho_0 = \rho_{mf}/E$. By the Pi theorem, three non-dimensional groups are required to describe the system.

The non-dimensional group describing the initial geometry is given trivially by a = h_0/x_0. The effects of gravity and sedimentation can be accounted for by identifying their characteristic timescales :

$$t_{grav} = \frac{x_0}{\sqrt{gh_0}} \qquad t_{sett} = \frac{h_0}{V}\left(\frac{E-1}{E}\right) \tag{3}$$

which can be combined to form a non-dimensional group

$$N_{sett} = \left(\frac{t_{sett}}{t_{grav}}\right) \tag{4}$$

t_{grav} is the gravitational acceleration time (Figure 13a). t_{sett} is a hindered settling time and is the time necessary for sedimentation to take place were the expanded mixture allowed to settle in the reservoir (Appendix 2). The exact forms of these times are arbitrary, since each could be modified by a factor f(a), but they have been chosen for their clear physical significance. The values of t_{grav} in our experiments were 0.1-0.2 s, while those of t_{sett} were 3-9 s, so that the timescale of sedimentation was much longer than that of gravitational acceleration. Values of N_{sett} ranged between 10 and 50 (Figure 14a, b). Note that if the flow was not expanded (E = 1.00), then both t_{sett} and N_{sett} were zero.

In principle we would expect the existence of a third dimensionless parameter, N_{drag}, related to drag. By analogy with equation 4, this might involve a hypothetical time t_{drag}, the time for the flow to react to the drag forces exerted on it. However it is not possible to evaluate either t_{drag} or N_{drag} because the form of the drag function is unknown.

Equation 4 provides a means of assessing the influence of sedimentation on the flow dynamics. We attempt in particular to find a better collapse of the data than provided by geometry and gravity alone (Figure 13a). In Figure 14, we plot runout time (t_∞) non-dimensionally as a function of $N_{sett.}$ t_∞ is scaled using t_{grav}, but using t_{sett} would be equally valid. V was determined as a function of E from the 1-D collapse tests (equation 2) and used to calculate N_{sett} for the flows. The runout times for phase 3 collapse very well as (Figure 14)

$$\frac{t_\infty}{t_{grav}} \approx N_{sett}^{0.55} \qquad (5)$$

Runout times for phase 4 scale like equation 5, but with an exponent of ~ 0.58. The phase-3 runout distance x_∞, similarly collapses as (Figure 14)

$$\frac{x_\infty}{x_0} \approx \frac{1}{7.3a} N_{sett}^{1.02} \qquad (6)$$

Runout distances for phase 4 scale like equation 6, also with an exponent of ~1.02. Plotting the x-t data of Figure 4 as x/ x_∞ versus t/t_∞ (using equations 5 and 6 to calculate x_∞ and t_∞) yields a good collapse for all three primary flow phases (Figure 15).

Equations 5 and 6 are presented with some caution. While they appear to confirm that N_{sett} describes the role of sedimentation in the ash flows, the role of a remains less well defined. Aspect ratio was not varied greatly in our experiments, so we cannot be sure that the equations account accurately for the effects of initial geometry.

Taken at face value, however, equations 5 and 6 appear to describe (within the range of experimental parameters used) the full dynamics of the initially expanded ash flows using only two dimensionless numbers, neither of which includes drag. This can be interpreted in two ways. One is that the dynamics were indeed governed entirely by geometry, gravity and sedimentation, with no detectable dependence on drag. However, this seems physically implausible given the role that basal drag necessarily played during phase 3, as well as in reducing frontal velocity below the inviscid value in phase 2. The second possibility is that the effect of drag is somehow hidden in the equations. We intuitively prefer this second possibility and present a simple, but speculative explanation.

Rapidly flowing fluidized materials exhibit complex rheological behaviours. The vertical gas flux causes momentum transfer between particles and gas [*Eames and Gilbertson*, 2000]. This disrupts particle contact chains, causing an overall reduction of stresses and an increase in the proportion of stresses generated by particle collisions rather than friction [*Nott*

and Jackson, 1992]. Scaling of the phase 2 frontal velocities with $\sqrt{gh_0}$ is suggestive of a basal stress of the form T~cρu², where c is a constant. If so we can derive a dimensionless group characterizing drag, in the same way as sedimentation. If a volume of fluid, height h_0, length L, density ρ, and velocity u and subjected to a basal stress of this form, then the time t_{drag} for it to react to that stress and be brought to rest is given by the force balance $\rho u L h_0/t_{drag} \approx c\rho u^2 L$. Using $u \approx \sqrt{gh_0}$, this gives $t_{drag} \approx (1/c)\sqrt{h_0/g} = a\,t_{grav}/c$. We could therefore write a dimensionless drag number $N_{drag} = t_{sett}/t_{drag} = cN_{sett}/a$, which accounts for the drag but has the form $f(a,N_{sett})$. While we do not imply that this is an accurate description of the drag stress in our flows, it illustrates one way in which the effects of drag could plausibly be contained in equations 5 and 6.

Equation 6 accounts empirically for the strong dependence of flow runout on E and the weak dependence on h_0 (Figure 6a). Over the range of experimental conditions x_∞ as predicted by equation 6 varies by a factor of 2.0 due to E, but a factor of only 1.2 due to h_0. We can also use it to derive an approximate expression for the deposit aspect ratio, $\bar{h}_\infty / x_\infty$, where $\bar{h}_\infty$ is the mean deposit thickness. Since by volume conservation $\bar{h}_\infty (x_\infty + x_0) \approx x_0 h_0 / E$, we can write $\bar{h}_\infty / x_\infty \approx x_0 h_0 / E x_\infty (x_\infty + x_0)$. Expansion of this expression shows that it depends only very weakly on h_0, explaining why h_0 has little effect on deposit aspect ratio within the range of experimental parameters (Figure 10).

Comparison with other types of dam-break flow

The runout behaviour of our ash flows was similar in two important respects to other types of dam-break flow, including inviscid Newtonian fluids [*Rottman and Simpson*, 1983; *Simpson,* 1997; *Hogg,* 2006], dry granular materials in which the interstitial gas plays no role [*Lube et al.*, 2004; 2005; *Lajeunesse et al.,* 2004; 2005], and gas-fluidized glass beads [*Roche*

et al., 2002; 2004; 2005]. Transport in all these systems is dominated by a phase of approximately constant velocity, preceded by a brief acceleration phase and terminated by a brief stopping phase. Moreover, the constant velocity scaled as $\sqrt{gh_0}$, reflecting a balance of gravity and inertia during that phase of motion.

The distinguishing feature of our ash flows is, however, the important role played by sedimentation, which occurred because the ash was initially expanded by as much as 45% above its loose-packed state. Consequently deposition took place continuously at an expansion-dependent rate, causing the flows to thin progressively until they ran out of volume. In this respect our experiments contrast with the fluidized flows of *Roche et al*. [2002; 2004], the glass beads of which expanded by no more than 7-8% in the non-bubbling state.

Interestingly, observations show that even unsteady dry granular flows develop basal static zones that accrete with time [*Lajeunesse et al.,* 2005; *Lube et al*., 2005], so that deposition also occurs progressively in such flows. The difference is that in our ash flows the rate of deposition is a function of the expansion, whereas is dry granular flows it depends only on gravity and geometry. The results of the present study may help better understand the process of deposition and friction acquisition in these other types of rapid granular flow.

Hindered settling in pyroclastic flows

Deposition by hindered settling probably occurs in dense pyroclastic flows generated from the initially expanded state or expanded during runout [*Branney and Kokelaar,* 2002]. The experiments are applicable only to flows capable of non-bubbling expansions of at least a few percent under vertical gas flow. The ability of pyroclastic flow materials to expand uniformly increases with increasing fines content [*Druitt et al.,* 2007], so the experiments are

most relevant to flows composed of a large fraction of ash, such as surge-derived pyroclastic flows [*Druitt et al.,* 2002] or ash flows that form fine-grained ignimbrites.

The experiments allow us to evaluate the effect of rapid horizontal shear on hindered settling. The settling velocities in our ash flows were found to be identical to those in 1-D bed-collapse tests at the same initial expansions, despite high rates of shear. This appears inconsistent, however, with a recent study by *Bareschino et al.* [2007], who studied hindered settling of volcanic ash in 1-D beds sheared between concentric vertical cylinders at rates of up to 30 s^{-1}. These authors found that shear significantly delayed hindered settling, resulting in t_{sett} values up to 7 times longer than in corresponding non-shearing beds, and they concluded that settling in rapid particulate shear flows would be slower than in quasi-static beds composed of the same materials.

These contrasting findings are probably due to the different shear modes of the two experimental systems. In the experiments of *Bareschino et al.* [2007], the shear planes were vertical, so that deformation persisted to the base of the bed, retarding hindered settling immediately above the depositional interface. Sediment aggradation in our experiments took place below a horizontal shear flow with a no-slip basal condition. Our result can be understood if, like velocity, the shear rates in our flows declined to zero at the flow-sediment interface. Deposition would have consequently taken place under quasi-static conditions, even though the overriding flow was shearing rapidly.

We conclude that shear has no effect on deposition rates under horizontal shear flows, offering a possible way of incorporating hindered settling into models of dense pyroclastic flows. Note that the shear rates in our experiments (up to 80 s^{-1}) were probably higher than those in real pyroclastic flows; for example, the mean velocity gradient in a pyroclastic flow 2m thick travelling at 10 m s^{-1}, (e.g., *Druitt et al.,* [2002]) would be only ~ 5 s^{-1}. Application of these concepts to the natural system requires caution, however; deposition rates from

pyroclastic flows may depend critically on fluxes of entrained or internally generated gas, and on the variation of those fluxes with time during transit. However once gas sources have ceased to be effective, deposition by hindered settling should proceed at the rates predicted by this present study.

Conclusions

We have carried out experiments on rapid shear flows of volcanic ash using a lock-exchange flume. The ash was heated to 170 ° C to avoid the cohesive effects of moisture, then expanded by fluidization in the non-bubbling state by various amounts up to 43 %. Once released, the ash formed shallow, unsteady flows that defluidized progressively as they travelled down the flume. No measurable particle size segregation took place, allowing us to assign bulk properties to the ash and analyse the results quantitatively. The flows slid against the walls of the flume with thin boundary layers. Flow was laminar, with no large-scale turbulent motions.

The flows exhibited the three emplacement stages typical of other types of lock-exchange flows. Following a brief initial phase of rapid ~ 1g acceleration (phase 1), the flow fronts attained an approximately constant velocity that was maintained for most of the runout (phase 2). The phase-2 velocity scaled as $\sqrt{gh_0}$, implying a balance between gravity and inertial forces. Drag forces then brought the flow front to a halt during a brief stopping phase (phase 3).

Deposition from the flows took place continuously at a rate independent of distance down the flume but dependent on the initial expansion. This caused the flows to get progressively thinner until they ran out of volume. Despite high rates of shear, the rates of deposition were indistinguishable from those measured in quasi-static beds under the same conditions of initial expansion, possibly because the shear rate in the flows declined to zero at the depositional

interface. It may therefore be possible to incorporate quasi-static measurements of deposition rates into mathematical models of particulate shear currents like pyroclastic flows.

While the phase 1 flow motions of the ash flows were governed entirely by initial geometry and gravity, the roles played by sedimentation and drag were non-negligible in phase 2 and dominant in phase 3. The dynamics could be described to a first approximation by two non-dimensional groups: one describing initial flow geometry, and the other being a ratio of the characteristic timescales of particle settling and gravity. An apparent lack of dependence on drag forces may be an artefact of their inertial nature.

Acknowledgments

We thank J. L. Fruquière and E. Brut for technical assistance throughout the project. Richard Iverson and Jim Vallance provided helpful reviews.

Appendix 1. Correction of 1-D hindered settling velocities

Collapse tests can be carried out in two different configurations. In one (single drainage), cutting the gas supply isolates gas trapped in the windbox, which is then vented upwards through the bed. In the second configuration (dual drainage), gas from the bed escapes downwards through the base of the windbox, as well as upwards through the bed [*Park et al.*, 1991; *Lettieri et al.,* 2000]. The present experiments were carried out in single-drainage mode. One-dimensional hindered settling velocities measured in single-drainage mode are underestimated because the windbox contents are evacuated through the collapsing bed. *Tung and Kwauk* [1982] provided a simple analysis of this effect, in which the apparent (measured) settling velocity is given by

$$V_{app} = V_{hs} - U_{dist} \ , \qquad \text{(A1)}$$

where V_{hs} is the true settling velocity, and U_{dist} is the upwards-directed gas velocity through the distributor plate due to windbox evacuation. Assuming that the leakage rate is constant over a duration t_{leak}, U_{dist} is given by :

$$U_{dist} = \left(\rho_{mf}\, g h_{mf} + \Delta P_{dist}\right) \frac{h_w}{P_a\, t_{leak}}. \qquad \text{(A2)}$$

where ρ_{mf} and h_{mf} are the bulk density and height of the settled bed, ΔP_{dist} is the pressure drop across the distributor plate, h_w is the height of the windbox, and P_a is atmospheric pressure. In our system ΔP_{dist} is much smaller than $\rho_{mf} g h_{mf}$, and can be neglected. If t_{leak} is assumed to equal the collapse duration, the equations can be solved for V_{hs} [*Tung and Kwauk,* 1982; *Geldart and Wong,* 1985].

Application of the equations to the results of Figure 2a shows that settling velocity is underestimated by factors of ~ 10 % at E = 1.10 and ~ 2 % at E = 1.43, which are comparable to, or smaller than, the measurement error. More detailed procedures have been developed by *Park et al.* [1991] and *Cherntongchai and Brandani* [2005], but they do not change the order of magnitude of the correction.

Appendix 2. Hindered settling and deposit aggradation

Consider a one-dimensional bed of height h_0 and particle concentration C_0 expanded by a fraction E, where $E = h_0/h_{mf}$, and h_{mf} is the non-expanded height at minimum fluidization. By mass conservation, the suspension concentration is

$$C_0 = \frac{C_{mf}}{E}, \qquad \text{(A3)}$$

If the suspension re-sediments with a hindered settling velocity V(E), the sediment aggradation velocity is

$$S = \frac{CV}{(C_0 - C)} = \frac{V}{(E-1)} \qquad \text{(A4)}$$

and the time for complete deposition of the bed is

$$t_{sett} = \frac{h_{mf}}{S} = \frac{h_0}{V}\left(\frac{E-1}{E}\right) \tag{A5}$$

The reader is referred to *Druitt et al.* [2007] for a full discussion of these processes.

References

Bareschino, P., T. Gravina, L. Lirer, A. Marzocchella, P. Petrosino, and P. Salatino (2007), Fluidization and de-aeration of pyroclastic mixtures: The influence of fines content, polydispersity and shear flow, *J. Volcanol. Geotherm. Res., 164*, 284-292.

Branney, M. J., and P. Kokelaar (2002), Pyroclastic density currents and the sedimentation of ignimbrites, *Geol. Soc. Lond., Memoirs*, *27*, 152 pp.

Bruni, G., P. Lettieri, D. Newton, and J. G. Yates (2006), The influence of fines size distribution on the behaviour of gas fluidised beds at high temperature, *Powder Technol., 163,* 88-97.

Cherntongchai, P., and S. Brandani (2005), A model for the interpretation of the bed collapse experiment, *Powder Technol.*, *151*, 37-43.

Davies, R., and B. Kaye (1971), Experimental investigation into the settling behavior of suspensions, *Powder Technol., 5,* 61.

Druitt, T. H. (1995), Settling behaviour of concentrated, poorly sorted dispersions and some volcanological applications. *J. Volcanol. Geotherm. Res., 65,* 27-39.

Druitt, T. H. (1998). Pyroclastic density currents. *In Gilbert, J. & Sparks, R. S. J. (eds) The physics of explosive volcanic eruptions. Geol. Soc. Lond. Special Publ., 145*: 145-182.

Druitt, T. H., E. S. Calder, P. D. Cole, G. E. Norton, L. J. Richie, R. S. J. Sparks, and B. Voight (2002), Small-volume, highly mobile pyroclastic flows formed by rapid sedimentation from pyroclastic surges at Soufrière Hills Volcano, Montserrat: an

important volcanic hazard, *In Druitt, T. H. & Kokelaar, B. P. (eds) The eruption of Soufrière Hills Volcano, Montserrat, from 1995 to 1999. Mem. Geol. Soc. London*, *21*, 263-281.

Druitt, T. H., G. Bruni, P. Lettieri, and J. G. Yates (2004), The fluidization behaviour of ignimbrite at high temperature and with mechanical agitation, *Geophys. Res. Lett.*, *31*, 10.1029/2003 GL018593.

Druitt, T. H., G. Avard, G. Bruni, P. Lettieri, and F. Maes (2007), Gas retention in fine-grained pyroclastic flow materials at high temperatures, *Bull. Volcanol.,* 10.1007/s00445-007-0116-7.

Eames, I. and M. Gilbertson (2000), Aerated granular flow over a rigid horizontal surface, *J. Fluid Mech.*, *424*, 169-195.

Fan, L. S., and C. Zhu (1998), Principles of gas-solid flows, *Cambridge University Press,* 557pp.

Geldart, D., and A. C. Y. Wong (1985), Fluidization of powders showing degrees of cohesiveness- II. Experiments on rates of de-aeration, *Chem. Engng. Sci.*, *40*, 653-661.

Gilbertson, M., and I. Eames (2003)**,** The influence of particle size on the flow of fluidized powders, *Powder Technol.*, *131*, 197-205.

Hoblitt, R. P. (1986), Observations of the eruptions of July 22 and August 7, 1980 at Mount St. Helens, Washington, *US Geol. Surv. Prof. Paper*, *1335*, 44pp.

Hogg, A. J. (2006), Lock-release gravity currents and dam-break flows, *J. Fluid Mech., 569,* 61-87.

Hogg, A. J., and D. Pritchard (2004) The effects of hydraulic resistance on dam-break and other shallow inertial flows, *J. Fluid Mech., 501,* 179-212.

Ishida, M. H., and T. Shirai (1980), The flow of solid particles in an aerated inclined channel, *Powder Technol.*, *27*, 7-12.

Lajeunesse, E., A. Mangeney-Castelnau, and J.–P. Vilotte (2004), Spreading of a granular mass on a horizontal plane *Phys. Fluids*, *16*, 2371-2381.

Lajeunesse, E., J. B. Monnier, and M. Homsy (2005), Granular slumping on a horizontal surface, *Phys. Fluids*, *17*, 103302 pp.1-15.

Levine, A. H., and S. W. Kieffer (1991) Hydraulics of the August 7, 1980, Pyroclastic flow at Mount St. Helens, Washington, *Geology, 19,* 1121-1124.

Lettieri, P., J. Yates, and D. Newton (2000), The influence of interparticle forces on the fluidization behaviour of some industrial materials at high temperature, *Powder Technol.*, *110*, 117-127.

Lockett, M. J. and H. M. Al-Habbooby (1974), Relative particle velocities in two-species settling, *Powder Technol.*, 10, 67-71.

Loughlin, S. C., E. S. Calder, A. B. Clarke, P. D. Cole, R. Luckett, M. Mangan, D. Pyle, R. S. J. Sparks, B. Voight, and R. B.Watts, (2002b), Pyroclastic flows and surges generated by the 25 June 1997 dome collapse, Soufrière Hills Volcano, Montserrat, *In Druitt, T. H. & Kokelaar, B. P. (eds) The eruption of Soufrière Hills Volcano, Montserrat from 1995 to 1999. Mem. Geol. Soc. London, 21,* 191-210.

Lube, G., H. E. Huppert, R. S. J. Sparks, and M. Hallworth (2004), Axisymmetric collapse of granular columns, *J. Fluid Mech.*, *508*, 175.

Lube, G., H. E. Huppert, R. S. J. Sparks, and A. Freundt (2005), Collapses of two-dimensional granular columns, *Phys. Rev.*, *72*, 041301.

Mangeney, A., P. Heinrich, and R. Roche (2000), Analytical solution for testing debris avalanche numerical models, *Pure Appl. Geophys., 157,* 1081-1096.

Mangeney-Castelnau, A., F. Bouchut, J. P. Vilotte, E. Lajeunesse, A. Aubertin, and M. Pirulli (2005), On the use of Saint Venant equations to simulate the spreading of a granular mass, *J. Geophys. Res., 110*, B09103, doi:10.1029/2004JB003161.

Nezzal, A., J. F. Large, and P. Guigon (1998), Fluidization behaviour of very cohesive powders under mechanical agitation, Fluidization VIII, Proceedings of the Eighth Engineering Foundation Conference on Fluidization, May 14-19, *Am. Inst. Chem. Eng.*, pp. 77-82.

Nott, P., and R. Jackson (1992), Frictional-collisional equations of motion for granular materials and their applications to flow in aerated chutes, *J. Fluid Mech., 241*, 125-144.

Park, J. J., J. H. Park, I. S. Chang, S. D. Kim, and C. S. Choi (1991), A new bed-collapsing technique for measuring the dense phase properties of gas-fluidized beds, *Powder Technol.*, *66*, 249-257.

Richardson, J. F., and W. N. Zaki (1954), Sedimentation and fluidization: Part I. *Trans. Inst. Chem. Eng.*, *32*, 35-52

Rhodes, M. (1998), Introduction to particle technology, John Wiley and Sons, *48*, 89-94.

Roche, O., M. A. Gilbertson, J. C. Phillips, and R. S. J. Sparks (2002), Experiments on deaerating granular flows and implications for pyroclastic flow mobility, *Geophys. Res. Lett., 29*(16), 1792, doi:10.1029/2002GL014819.

Roche, O., M. A. Gilbertson, J. C. Phillips, and R. S. J. Sparks (2004), Experimental study of gas-fluidized granular flows with implications for pyroclastic flows emplacement, *J. Geophys. Res.*, *109*, B10201, doi: 10.1029/2003JB002916.

Roche, O., M. A. Gilbertson, J. C. Phillips, and R. S. J. Sparks (2005), Inviscid behaviour of fines-rich pyroclastic flows inferred from experiments on gas-particle mixtures, *Earth. Planet. Sci. Lett.. 240,* 401- 414.

Rottman, J. W., and J. E. Simpson (1983), Gravity currents produced by instantaneous release of a heavy fluid in a rectangular channel, *J. Fluid Mech.*, *135*, 95-110.

Simpson, J. E. (1997), Gravity Currents in the Environnement and the Laboratory, *2nd Ed., Cambridge Univ. Press.*, New York.

Sparks, R. S. J. (1976), Particle size variations in ignimbrites and implications for the transport of pyroclastic flows, *Sedimentology*, *23*, 147-188.

Sparks, R. S. J. (1978), Gas release rates from pyroclastic flows: An assessment of the role of fluidization in their emplacement, *Bull. Volcanol., 41*, 1-9.

Takahashi, T., and H. Tsujimoto (2000), A mechanical model for Merapi-type pyroclastic flow, *J. Volcanol. Geotherm. Res., 98*, 91-115.

Tung, Y., and M. Kwauk (1982). Fluidization science and technology, Gordon and Breach, New York, p155.

Wilson, C. J. N. (1980), The role of fluidization in the emplacement of pyroclastic flows: an experimental approach, *J. Volcanol. Geotherm. Res., 8*, 231-249.

Figure captions

Figure 1. (a) Experimental system and parameter definitions. Note that frontal distance x_f down the flume is defined as zero at the reservoir lock gate. (b) Detailed anatomy of the high-temperature lock-exchange flume. (1) Rotameters. (2) Three-way valve. (3) Evacuation pipe. (4) Windbox. (5) Heating mats. (6) Lock-gate reservoir. (7) Temperature controller-regulator. (8) Thermocouple. (9) Pressure transducer. (10) Sliding lock gate. (11) Horizontal flume. (12) Recuperation box.

Figure 2. (a) Data pertaining to the 1-D expansion and settling (bed-collapse) behaviour of the ash in the reservoir with the lock-gate closed. The two velocities shown are that required to expand the ash to a given value E, and that at which the expanded ash settled when the gas supply was turned off. (b) Values of hindered settling velocities in the moving ash flows determined from video footage, using the method described in the text and in Appendix 2. The grey area covers the 1-D data of (a).

Figure 3. (a) Release of a moderately expanded ash flow (E = 1.17, set 2). (b) Wedge-shaped front of a weakly expanded flow (E = 1.07, set 2). (c) Rounded front of a strongly expanded flow (E = 1.35, set 2). (d) Surface instabilities formed during propagation of a moderately expanded flow (E = 1.17, set 2). (e) Propagation of the secondary wave (phase 4) across the distal limit of the already-deposited primary flow, viewed from above (1.10, set 2).

Figure 4. Flow frontal position versus time for (a) set 1 and (b) set 2.

Figure 5. Flow aspect ratio (mean height / instantaneous length) versus time for (a) set 1 and (b) set 2. The mean flow height was obtained by measuring the cross-sectional area of the flow and dividing by the flow length. The grey area in (b) is the data coverage in (a).

Figure 6. Variation of (a) runout distance, (b) runout duration, and (c) mean phase-2 velocity as functions of initial expansion.

Figure 7. (a) Variation of x_2 (the distal limit of flow phase 2) and x_e (the distal limit of the lower strandline) as functions of initial expansion. x_e is a measure of the distance to which the ash flows remained in the expanded state during transit. (b) The same parameters expressed as fractions of x_3, the total phase-3 runout distance of the primary flow.

Figure 8. (a) Vertical view of an ash flow surface laced with tracer particles (pumices, shown as rectangles) showing the absence of surface vorticity. (b) Surface velocities for the labelled time intervals, calculated from the data in (a). The flow slid against the flume walls, with boundary layers < 1 cm wide, except during phase 3 (interval t_5-t_4), when they grew to several cm in width. The data are for a flow initially expanded by 10 % (E = 1.10; set 2).

Figure 9. Profiles of the deposits from the experimental ash flows.

Figure 10. Deposit aspect ratio (mean thickness / phase-4 length) as a function of initial flow expansion for the two sets of experiments.

Figure 11. Upper strandline, lower strandline and deposit profiles for three ash flows (E = 1.07, 1.17, 1.43) of set 2.

Figure 12. Variation of estimated hindered settling velocity with distance from the lock gate for a moderately expanded ash flow (E = 1.17, set 2).

Figure 13. (a) Data of Figure 4 plotted non-dimensionally using the scalings previously established for inviscid Newtonian fluids and fluidized flows of glass beads. (b) Non-dimensional phase-2 velocity as a function of initial expansion.

Figure 14. Logarithmic plots of t_∞/t_{grav} and x_∞/x_0 versus N_{sett} for flow phases 3 and 4, where the values of t_∞ and x_∞ are calculated using equations 5 and 6 respectively.

Figure 15. Collapse of the x-t data of Figure 4 using the scalings of equations 5 and 6.

Table 1: Grain-size evolution of the ash sample over the duration of the experiments

Grain size (μm)	250	180	125	90	< 63
1-D Study (wt %)[1]	8.2	12.4	14.4	18.7	46.3
Exp 1 (wt %)[2]	8.4	12.3	14.4	18.7	46.2
Exp 18 (wt %)[2]	8.4	12.3	14.3	18.7	46.3

[1] 1-D expansion and collapse tests carried out at the start of the study

[2] Flume experiment (exp 1 being the first and exp 18 being the last)

Figures

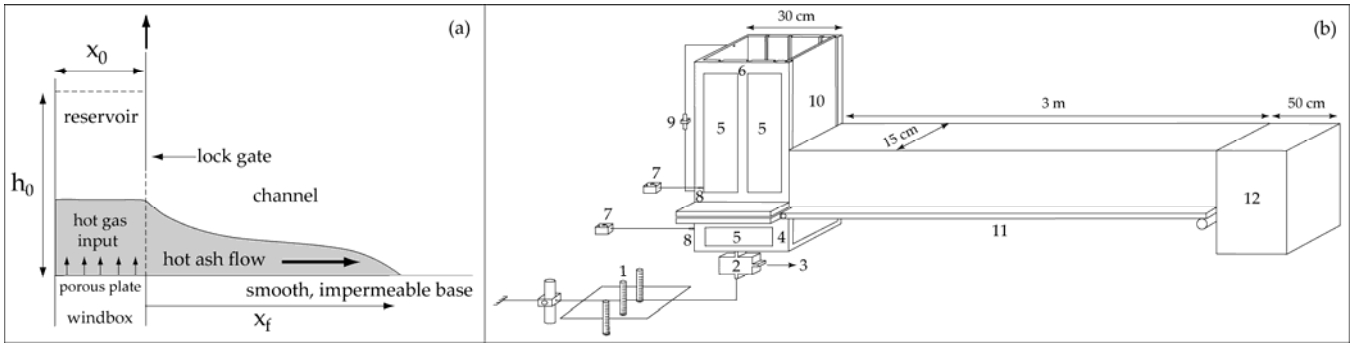

Figure 1

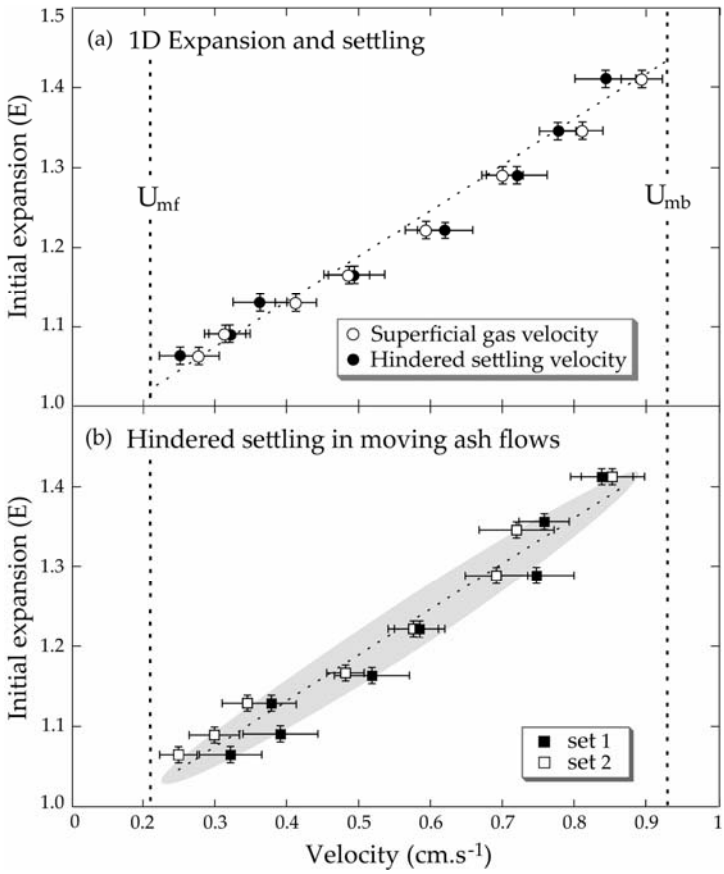

Figure 2

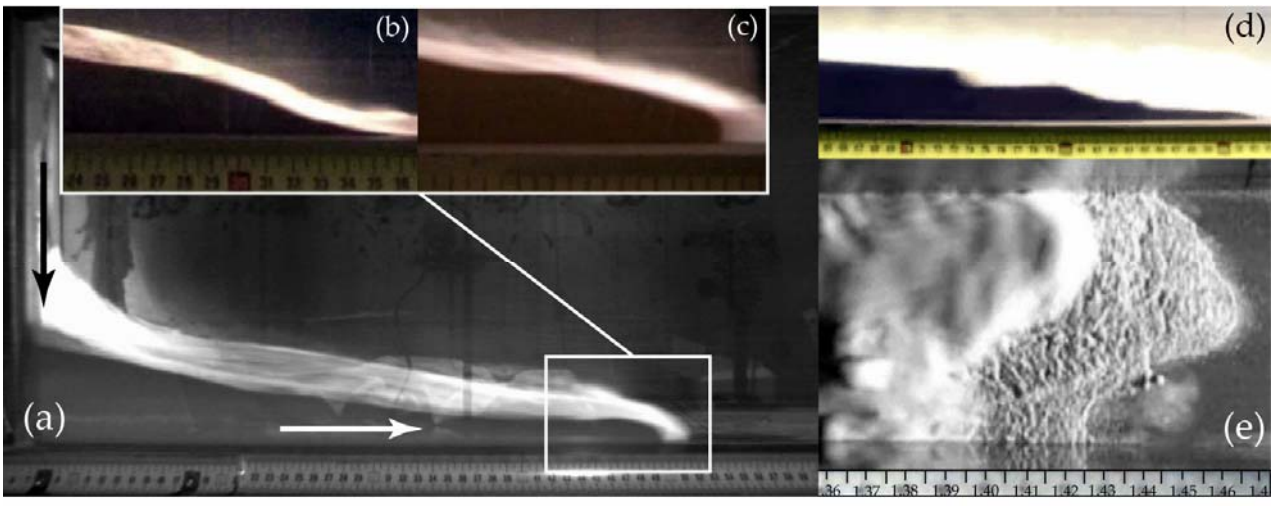

Figure 3

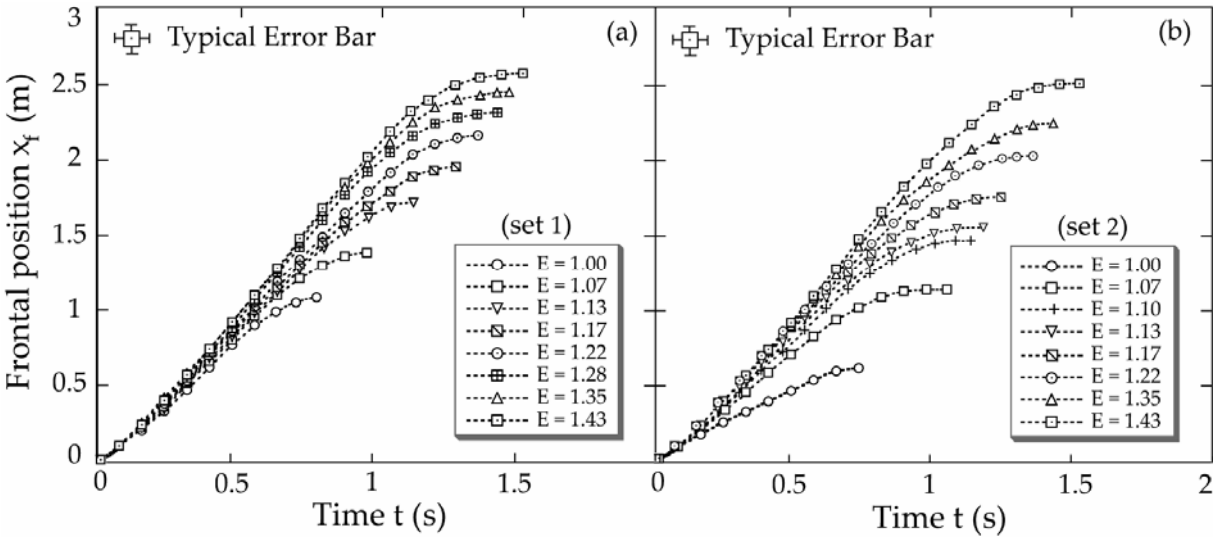

Figure 4

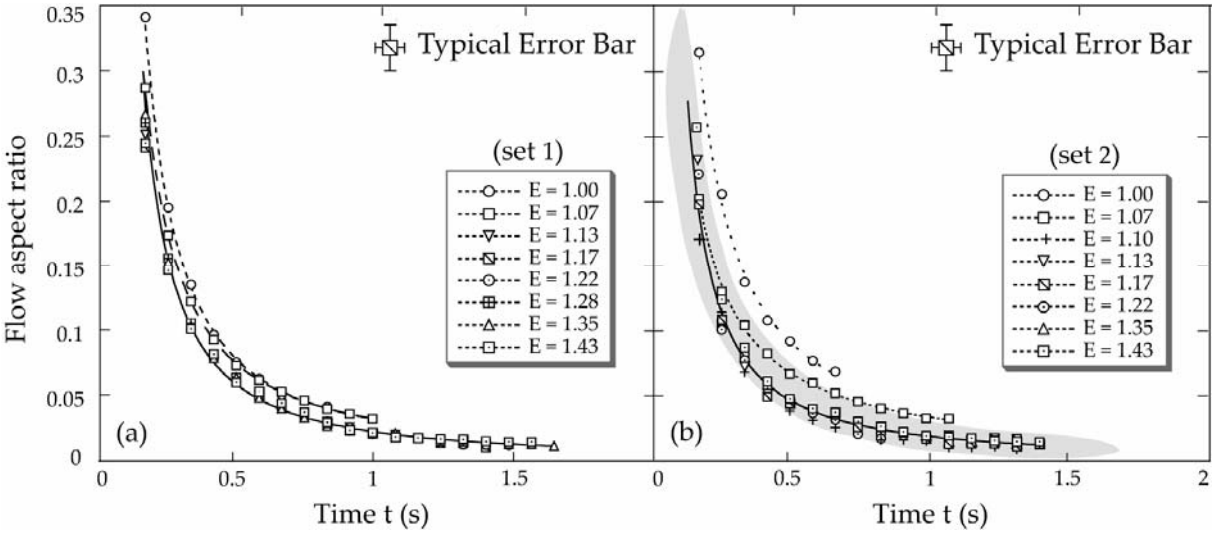

Figure 5

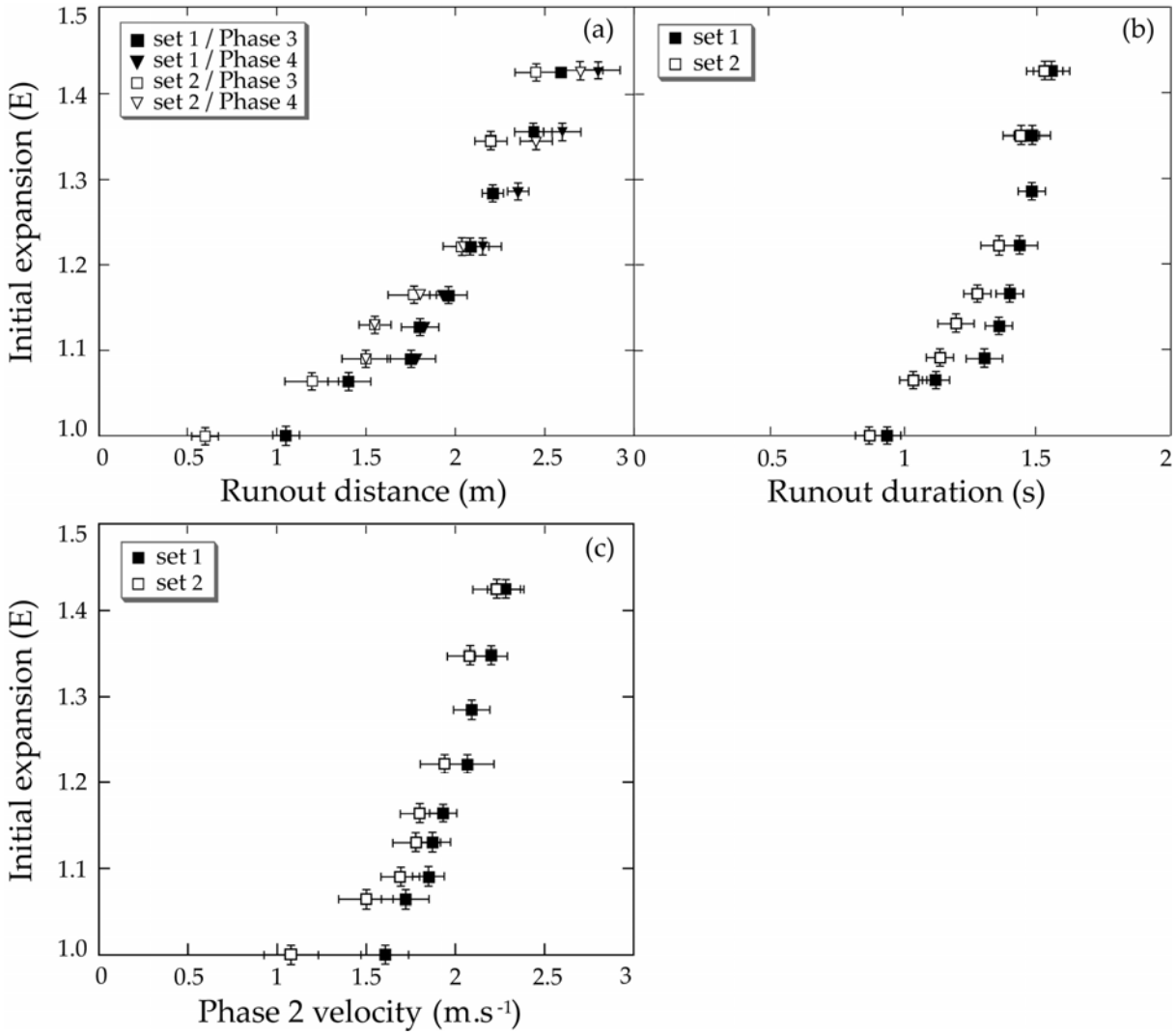
(a)
set 1 / Phase 3
set 1 / Phase 4
set 2 / Phase 3
set 2 / Phase 4
Initial expansion (E)
Runout distance (m)
(b)
set 1
set 2
Runout duration (s)
(c)
set 1
set 2
Initial expansion (E)
Phase 2 velocity (m.s-1)

Figure 6

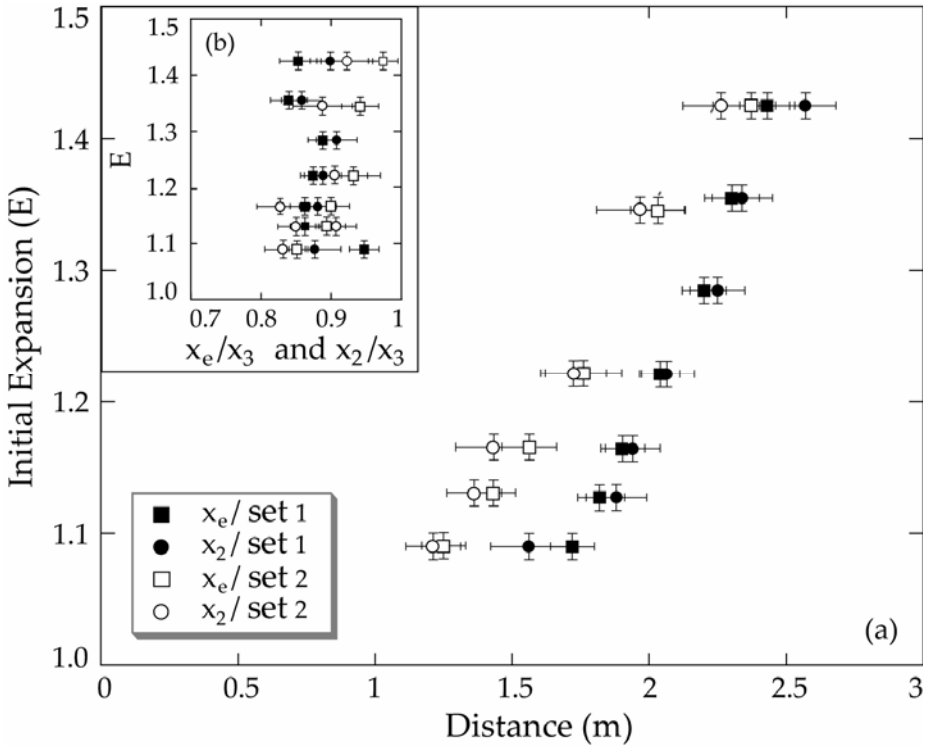

Figure 7

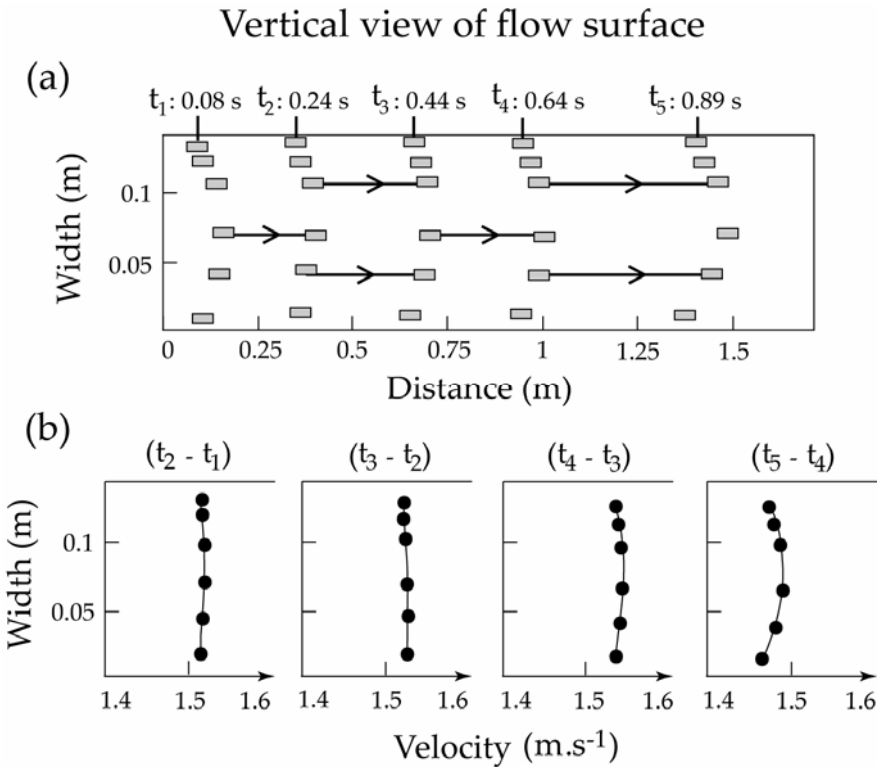

Figure 8

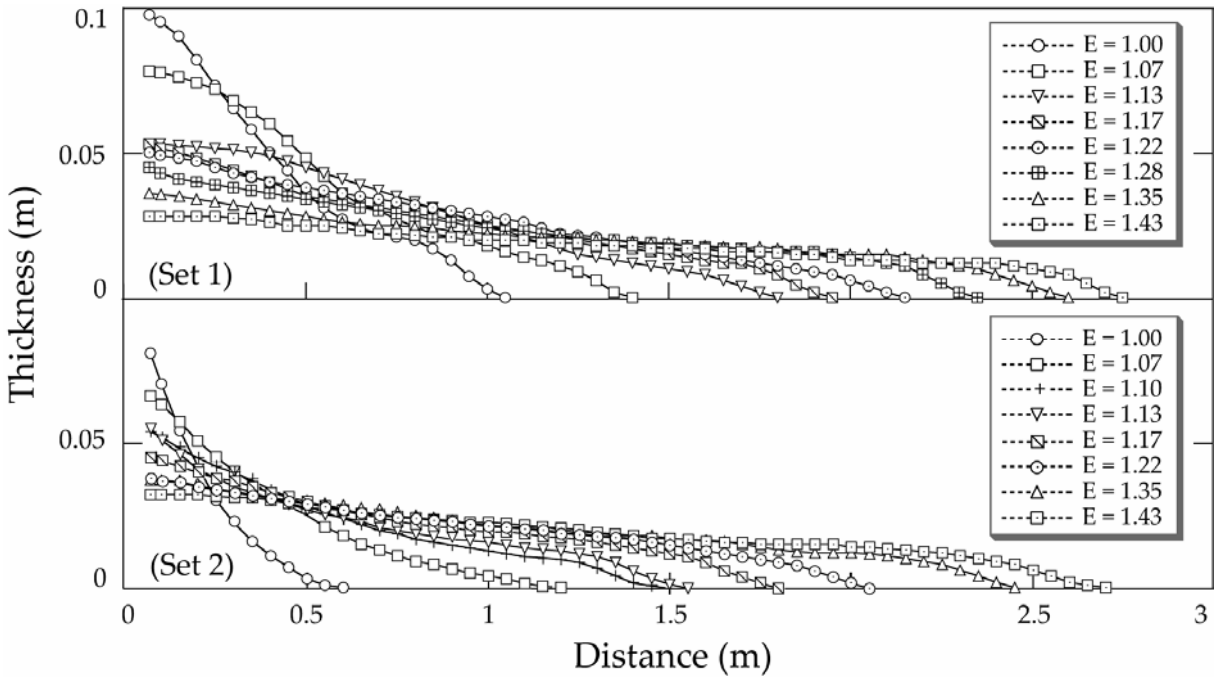

Figure 9

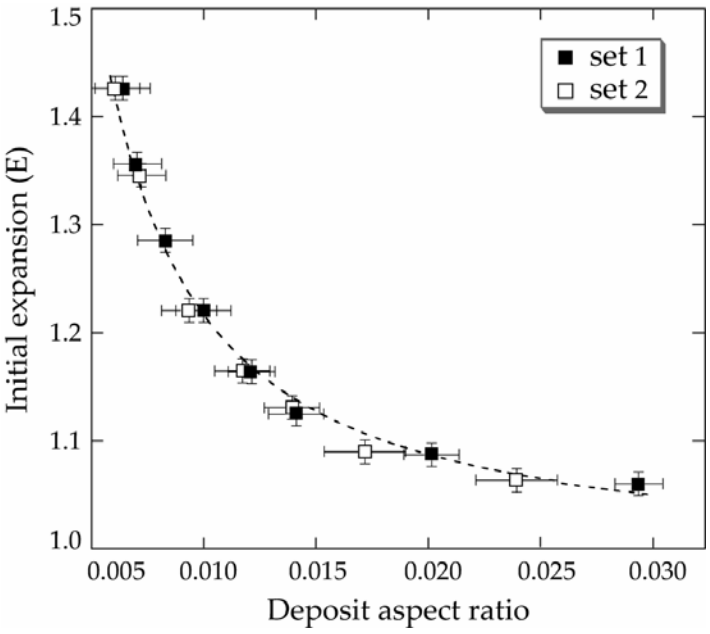

Figure 10

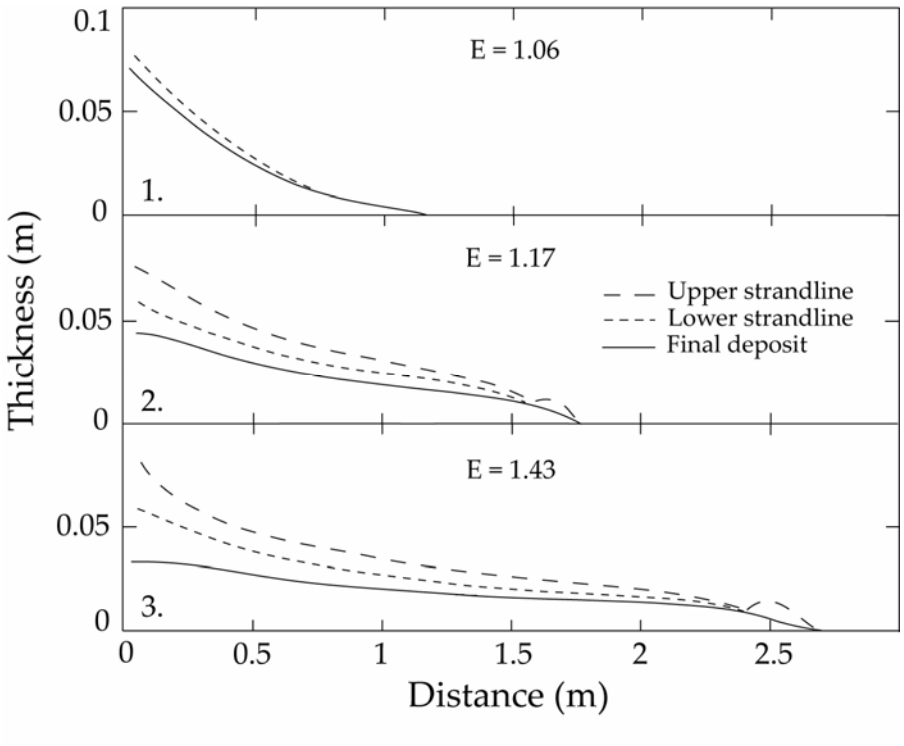

Figure 11

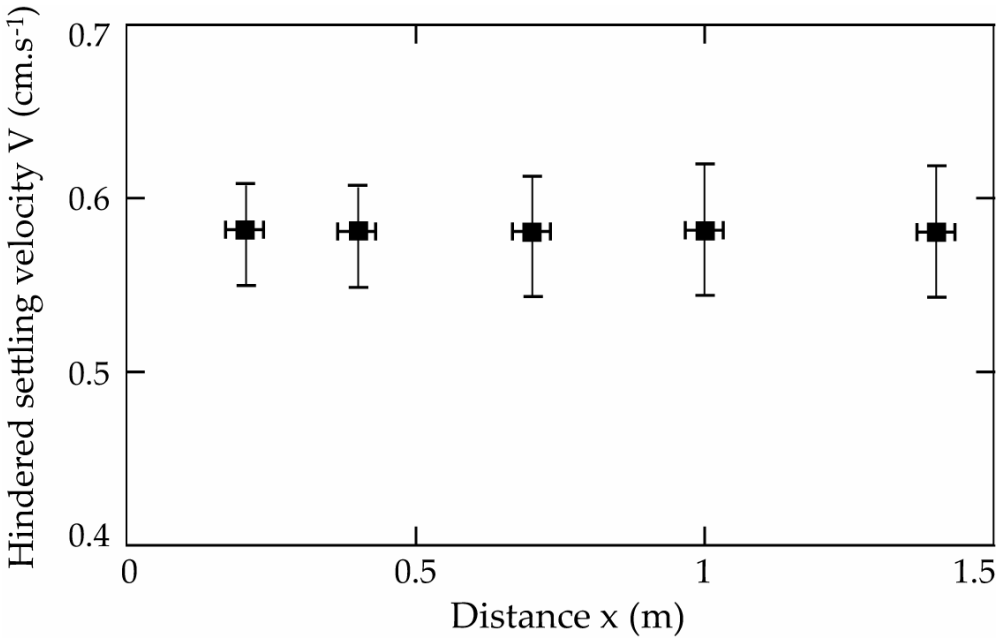

Figure 12

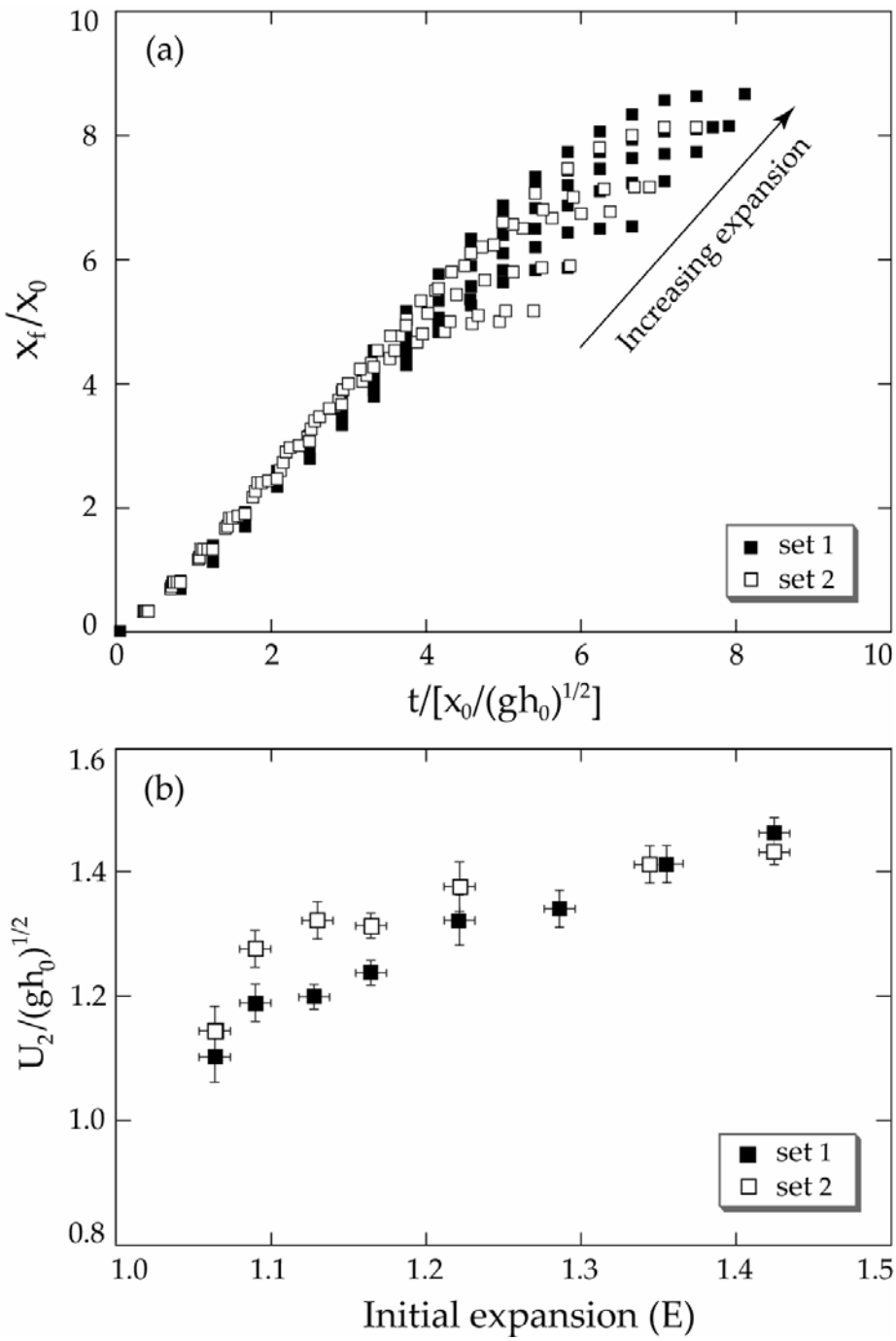
(a)
x_f/x_0
$t/[x_0/(gh_0)^{1/2}]$
Increasing expansion
set 1
set 2
(b)
$U_2/(gh_0)^{1/2}$
Initial expansion (E)
set 1
set 2

Figure 13

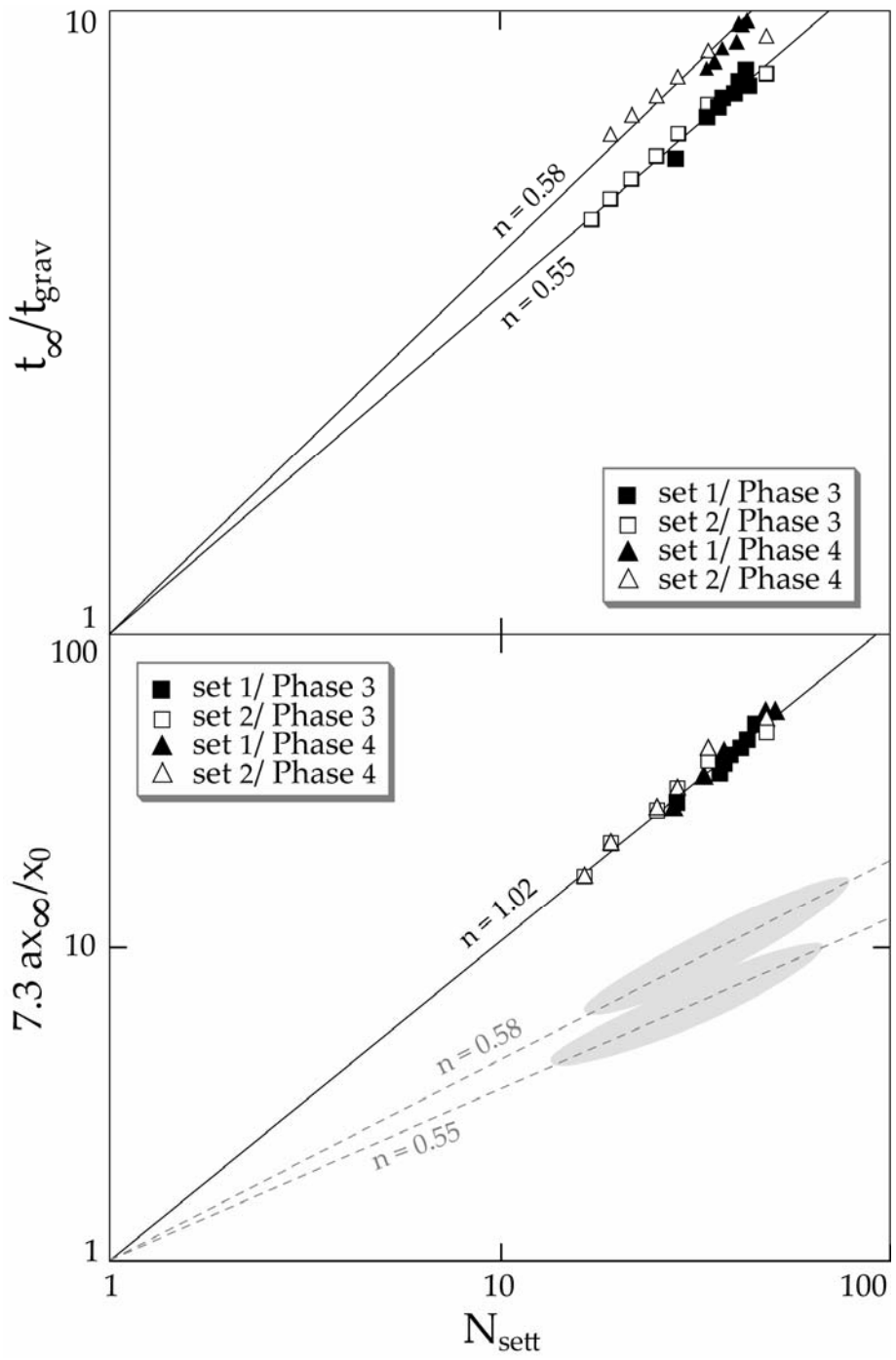
10
1
t_∞/t_{grav}
n = 0.58
n = 0.55
set 1/ Phase 3
set 2/ Phase 3
set 1/ Phase 4
set 2/ Phase 4
100
10
1
$7.3\ ax_\infty/x_0$
n = 1.02
n = 0.58
n = 0.55
1
10
100
N_{sett}

Figure 14

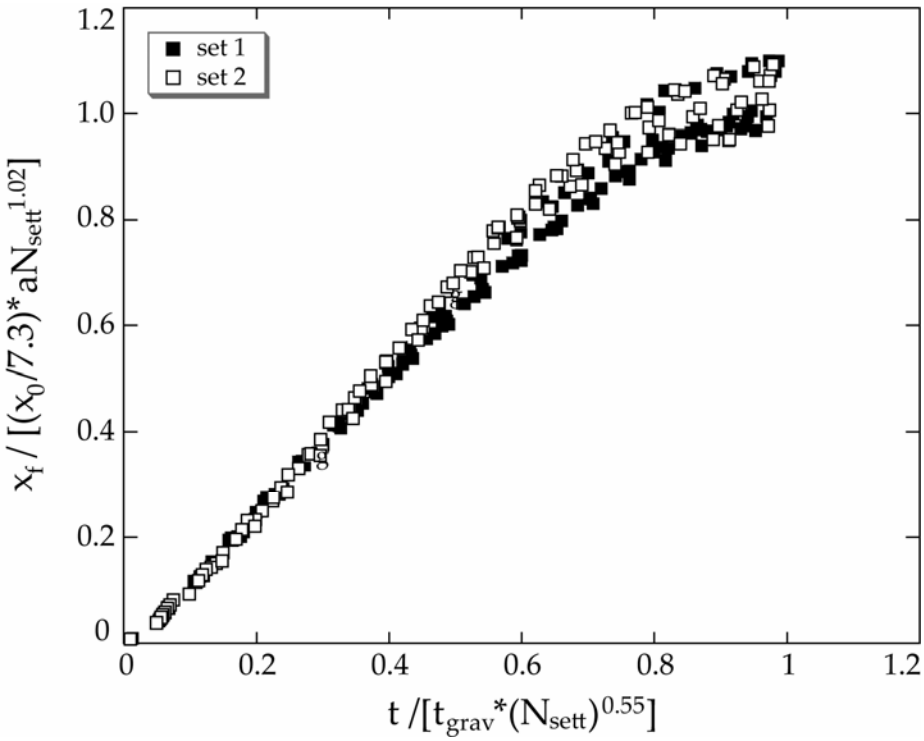
set 1
set 2
1.2
1.0
0.8
0.6
0.4
0.2
0
0
0.2
0.4
0.6
0.8
1
1.2
$x_f / [(x_0/7.3)^* aN_{sett}^{1.02}]$
$t /[t_{grav}^*(N_{sett})^{0.55}]$

Figure 15